X043

Least-squares Reverse-time Migration

G. Yao* (Imperial College London) & H. Jakubowicz (Imperial College London)

SUMMARY

Migration attempts to produce an image of the subsurface by reversing the propagation effects in seismic data. Although in principle this requires the inverse of a modelling operator, in practice the adjoint of the modelling operator is used instead. In cases where the data are subject to significant aliasing, truncation, noise, or are incomplete, the adjoint of a modelling operator is not a good approximation to the inverse, and this degrades the resolution of the final migrated image.

An improved approximation to the inverse operator can be obtained using a least-squares approach. In this work we present a least-squares formulation of reverse-time migration scheme that is based on an explicit matrix representation of generalised diffraction-stack migration. Our implementation uses a modified source wavelet to perform the forward and inverse steps at each iteration, and is regularised using a roughness penalty constraint. The results show increased resolution compared to conventional reverse-time migration.

Introduction

Migration attempts to produce an image of the subsurface by reversing the propagation effects in seismic data. In principle, this requires the inverse of a modelling operator, but in practice the adjoint of the modelling operator is used instead. This applies to nearly all migration methods, including reverse-time migration (RTM). In cases where the data are subject to significant aliasing, truncation, noise, or are incomplete, the adjoint of a modelling operator is not a good approximation to the inverse (Claerbout, 2004). This then degrades the resolution of the final migrated image.

An improved approximation to the inverse-modelling/migration operator can be obtained by formulating the migration process as a least-squares problem (Nemeth et al., 1999; Kühl and Sacchi, 2001; Kaplan et al., 2010). In this work we describe a least-squares implementation of RTM. Our method is based on the generalised diffraction-stack migration formulation of Schuster (2002). It uses a modified source wavelet to perform the forward and inverse steps at each iteration, and includes a roughness constraint to regularise the least-squares calculation.

Theory

Migration consists of three steps: forward modelling of the source wavefield, back propagation of the recorded data, and imaging. In RTM forward modelling is achieved by solving the two-way wave equation, and, for a point source, can be expressed as

$$u_s(\boldsymbol{x}, \omega) = G(\boldsymbol{x}|\boldsymbol{x_s}; \omega)\, S(\omega)\,, \qquad (1)$$

where u_s is the modelled wavefield, G is the Green's function, S is the source signature, $\boldsymbol{x}$ is position, $\boldsymbol{x_s}$ is the source location, and ω is angular frequency. The recorded data, R, are then back-propagated into the subsurface using the adjoint of the modelling operator, $G^\dagger$, giving

$$u_r(\boldsymbol{x}, \omega) = \int G^\dagger(\boldsymbol{x}|\boldsymbol{x_r}; \omega)\, R(\boldsymbol{x_r}, \omega)\, d\boldsymbol{x_r}. \qquad (2)$$

The imaging step generates the reflectivity, $I(\boldsymbol{x})$, by relating u_s and u_r to each other at all points in the subsurface. This is normally done by correlating the wavefields and selecting the zero lag, and can be expressed in the frequency domain as

$$I(\boldsymbol{x}) = \int u_s(\boldsymbol{x}, \omega)\, u_r^\dagger(\boldsymbol{x}, \omega)\, d\omega, \qquad (3)$$

where $u_r^\dagger$ is the conjugate (time-reverse) of the back-propagated data. Substituting Equations 1 and 2 into Equation 3 then gives the basic equation of RTM:

$$I(\boldsymbol{x}) = \iint [G(\boldsymbol{x}|\boldsymbol{x_s}; \omega)\, S(\omega)\,][G^\dagger(\boldsymbol{x}|\boldsymbol{x_r}; \omega)\, R(\boldsymbol{x_r}, \omega)]^\dagger\, d\omega\, d\boldsymbol{x_r}. \qquad (4)$$

Since $I(\boldsymbol{x})$ is real, Equation 4 can be rewritten as

$$I(\boldsymbol{x}) = \iint [G(\boldsymbol{x}|\boldsymbol{x_s}; \omega)\sqrt{S(\omega)}]^\dagger\, [G(\boldsymbol{x}|\boldsymbol{x_r}; \omega)\sqrt{S(\omega)}\,]^\dagger R(\boldsymbol{x_r}, \omega)\, d\omega\, d\boldsymbol{x_r}. \qquad (5)$$

Equation 5 can be implemented as follows: first, calculate the contributions from the Green's functions and source terms by solving the two-way wave equation using a source with a signature corresponding to $\sqrt{S(\omega)}$; next, evaluate the kernel in Equation 5 by conjugating and multiplying (i.e. time-reversing and convolving) the terms in square brackets (obtained from the first step), and then multiplying (convolving) the result with the recorded data; finally, sum all the traces and frequencies. This is the same as generalised diffraction-stack migration, and is equivalent to RTM (Schuster, 2002).

Equation 5 uses adjoints of forward-modelling operators, rather than inverse operators, and only provides an estimate of the subsurface reflectivity. By comparison, the recorded data correspond to the true reflectivity, $M(\boldsymbol{x})$, and can be described by

$$R(\boldsymbol{x_r}, \omega) = \iint [G(\boldsymbol{x}|\boldsymbol{x_s}; \omega)\sqrt{S(\omega)}][G(\boldsymbol{x}|\boldsymbol{x_r}; \omega)\sqrt{S(\omega)}\,]\, M(\boldsymbol{x})\; d\boldsymbol{x}. \qquad (6)$$

Equations 5 and 6 can be used to formulate an iterative least-squares scheme that produces an optimum estimate of the reflectivity consistent with the recorded data. This is done by minimising the objective function

$$F(I) = \| < R > - R \|^2, \qquad (7)$$

where $< R >$ represents the modelled data corresponding to the estimated reflectivity obtained from Equation (5), and R is the actual recorded data. The solution of Equation 7 forms the basis of the least-squares reverse-time migration (LSRTM) used here.

Implementation

Equation 7 can be solved using a modified conjugate-gradient method (Scales, 1987). Because of the structure of Equation 5, this algorithm can be implemented using matrices constructed directly from the forward-modelling operator and its adjoint, together with a modified source signature corresponding to $\sqrt{S(\omega)}$. This has the advantage of improving the efficiency of the calculation, and also ensures that the matrices satisfy the dot product test (Claerbout, 2004). As in the case of conventional RTM, the use of a two-way wave equation can produce low-wavenumber artefacts, but these can be removed using a Laplacian filter after migration. However, whereas the adjoint operator used in RTM is unconditionally stable, the inverse required for LSRTM can be ill-posed. This generates additional noise in the final result, but can be controlled using a roughness constraint in the objective function (Bube and Langan, 2008).

Examples

We will demonstrate our implementation of LSRTM using two models. The first model consists of nine point diffractors embedded in a medium with a constant velocity of 2000 m/s (Figure 1). Figure 4 shows a shot record from this model for a surface source at x=450 m, and receivers every 25 m along the surface; the source signature is a 30 Hz Ricker wavelet, and the direct arrivals, which do not contribute to imaging, have been removed. Figures 2 and 3 show the results of applying conventional RTM and LSRTM to the data in Figure 4, while Figures 5 and 6 show the modelled data corresponding to the RTM and LSRTM images. In this case noise and instabilities are not an issue, and Laplacian filtering is not required; the LSRTM result also does not use a roughness constraint.

Figures 1 to 6 show that RTM has two weaknesses relative to LSRTM. First, the diffractors in the RTM image have more sidelobes, and are less well-resolved than those from LSRTM. This is because the imaging condition for RTM is based on crosscorrelation, and preserves the imprint of the source signature in the migrated image. By comparison, in matching the image and recorded data, LSRTM compensates for the source signature. Second, the amplitudes of the later arrivals in the modelled RTM data are weaker than the corresponding events in the recorded data. This is due to the use of adjoint, rather than inverse, operators. In particular, the adjoint operators fail to correct adequately for geometrical spreading, and cause the forward-modelled and back-propagated wavefields to be weaker in the deeper parts of the model. The crosscorrelation imaging condition then compounds this problem since it multiplies the wavefields to give the final image. One way of avoiding this might be to use a deconvolution imaging condition (Valenciano and Biondi, 2003). However, in using an approximate inverse to describe the relationship between the image and recorded data, LSRTM provides a better representation of the amplitude effects related to propagation. This helps preserve the amplitudes inherent in the reflectivity, and leads to a more accurate image.

The second example uses the Marmousi synthetic dataset (Versteeg and Grau, 1991; Versteeg, 1993). Figure 7 shows the velocity model for the Marmousi data, while Figure 8 shows a shot record for a surface source location at x=3000 m, with receivers located between 425 m and 2800 m at intervals of 12.5 m. The RTM image from this shot record is shown in Figure 9, and corresponds to the area enclosed within the red box in Figure 7. In this case, low-wavenumber artefacts arising from the use of the two-way wave equation are an issue, but can be removed using a Laplacian filter (Figure 10). However, the final RTM image retains high-wavenumber artefacts (indicated by red arrows). Figure 11 shows the image produced by LSRTM without a roughness constraint. Relative to conventional RTM, this implementation of LSRTM suppresses high-wavenumber artefacts and increases the resolution in the final image, but also contains a significant amount of high-wavenumber noise. Figure 12 shows the corresponding LSRTM result, but with a roughness constraint. This successfully removes the high-wavenumber noise, but retains low-wavenumber artefacts from the solution of the two-way wave equation. Finally, Figure 13 shows the result of applying a Laplacian filter to the data in Figure 12. This image has fewer artefacts, is more highly resolved than that from RTM, and has more consistent amplitudes over a wider area. It demonstrates that LSRTM incorporating a roughness constraint can provide significant improvements over conventional RTM.

Conclusions

We have shown that LSRTM can be an effective method for imaging seismic data. Our implementation is based on generalised diffraction-stack migration with a modified source signature. This enables explicit matrices to be used for both the forward modelling and adjoint operators, providing improved efficiency and numerical accuracy. The method also incorporates a roughness constraint to regularise the least-squares optimisation and suppress high-wavenumber noise.

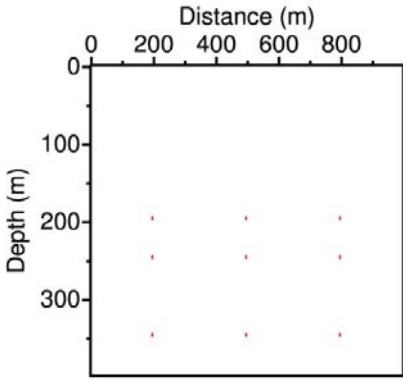

Figure 1 *Model*

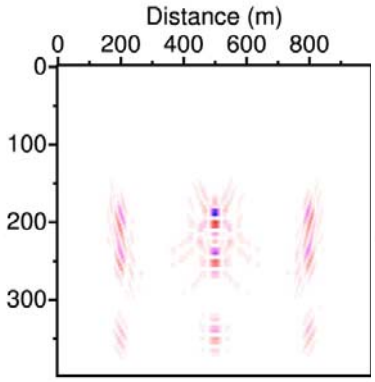

Figure 2 *RTM*

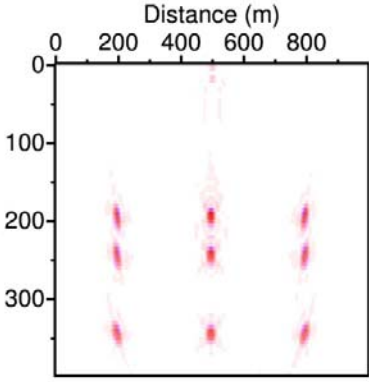

Figure 3 *LSRTM*

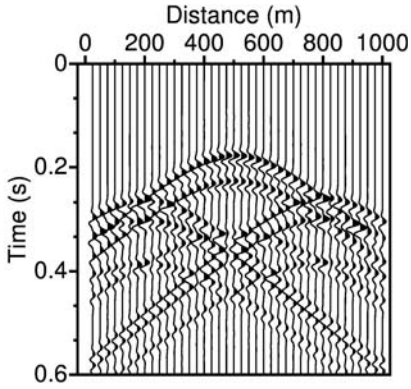

Figure 4 *Shot record*

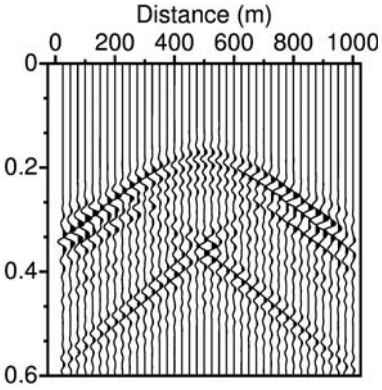

Figure 5 *RTM shot record*

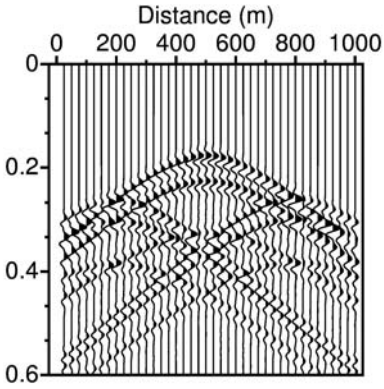

Figure 6 *LSRTM shot record*

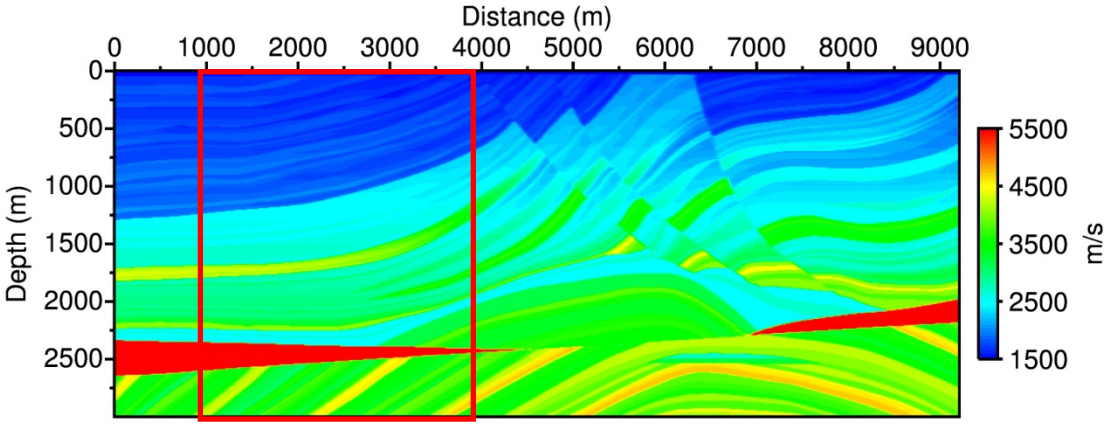

Figure 7 *Velocity model for the Marmousi synthetic dataset. The red box indicates the area covered by the migration of the shot record in Figure 8.*

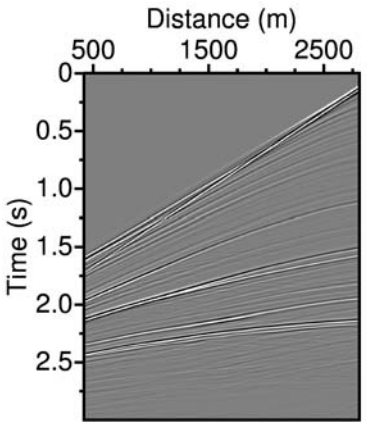

Figure 8 *Shot record from the Marmousi data*

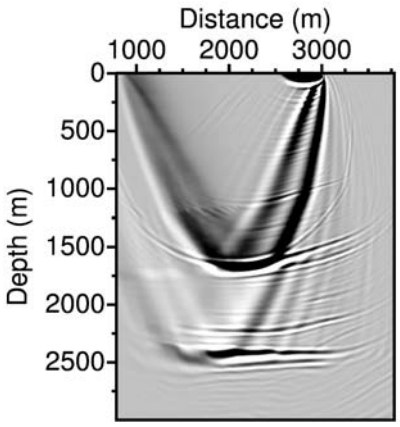

Figure 9 *RTM*

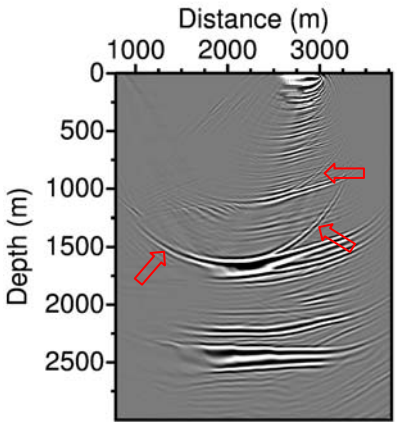

Figure 10 *RTM after Laplacian filtering*

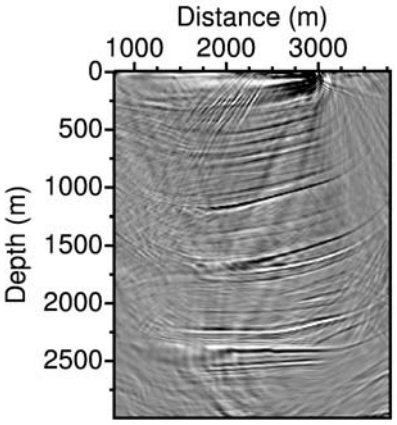

Figure 11 *LSRTM without a roughness constraint*

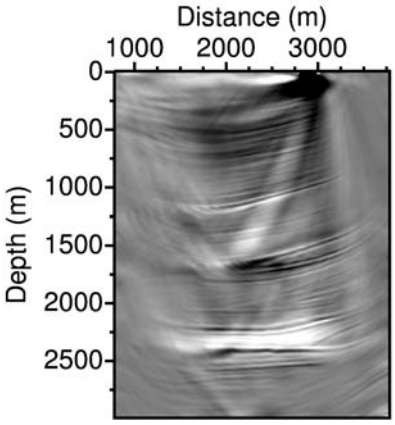

Figure 12 *LSRTM with a roughness constraint*

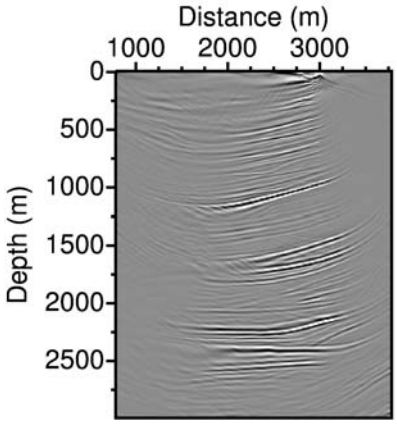

Figure 13 *LSRTM with a roughness constraint after application of a Laplacian filter*

References

Bube, K. P., and Langan, R.T., 2008, A Continuation Approach to Regularization of Ill-Posed Problems with Application to Crosswell-Traveltime Tomography. *Geophysics* **73**, VE337-VE351.

Claerbout, J.F., 2004, Earth Soundings Analysis: Processing Versus Inversion. *Blackwell Scientific Publications*.

Kaplan, S.T., Routh, P.S., and Sacchi, M.D., 2010, Derivation of Forward and Adjoint Operators for Least-Squares Shot-Profile Split-Step Migration. *Geophysics* **75**, S225-S35.

Kühl, H., and Sacchi, M.D., 2001, Generalized Least-Squares Dsr Migration Using a Common Angle Imaging Condition. *SEG Technical Program Expanded Abstracts* **20**, 1025-28.

Nemeth, T., Wu, C., and Schuster, G.T., 1999, Least-Squares Migration of Incomplete Reflection Data. *Geophysics* **64**, 208-21.

Scales, J.A., 1987, Tomographic Inversion Via the Conjugate Gradient Method. *Geophysics* **52**, 179-85.

Schuster, G.T., 2002, Reverse-Time Migration = Generalized Diffraction Stack Migration. *SEG Technical Program Expanded Abstracts* **21**, 1280-83.

Valenciano, A. A., and Biondi, B., 2003, 2-D Deconvolution Imaging Condition for Shot-Profile Migration. *SEG Technical Program Expanded Abstracts* **22**, 1059-1062.

Versteeg, R.J., and Grau, G. (eds.), 1991, The Marmousi experience. *Proc. EAGE workshop on Practical Aspects of Seismic Data Inversion (Copenhagen, 1990)*, EAGE, Zeist.

Versteeg, R.J., 1993, Sensitivity of prestack depth migration to the velocity model. *Geophysics* **58**, 873-882.